

Rearrangement of potassium ions and Kv1.1/Kv1.2 potassium channels in regenerating axons following end-to-end neurorrhaphy: ionic images from TOF-SIMS

Chiung-Hui Liu^{1,4} · Hung-Ming Chang³ · Tsung-Huan Wu¹ · Li-You Chen¹ · Yin-Shuo Yang¹ · To-Jung Tseng¹ · Wen-Chieh Liao^{1,2}

Accepted: 3 April 2017 / Published online: 12 April 2017
© Springer-Verlag Berlin Heidelberg 2017

Abstract The voltage-gated potassium channels Kv1.1 and Kv1.2 that cluster at juxtaparanodal (JXP) regions are essential in the regulation of nerve excitability and play a critical role in axonal conduction. When demyelination occurs, Kv1.1/Kv1.2 activity increases, suppressing the membrane potential nearly to the equilibrium potential of K^+ , which results in an axonal conduction blockade. The recovery of K^+ -dependent communication signals and proper clustering of Kv1.1/Kv1.2 channels at JXP regions may directly reflect nerve regeneration following peripheral nerve injury. However, little is known about potassium channel expression and its relationship with the dynamic potassium ion distribution at the node of Ranvier during the regenerative process of peripheral nerve injury (PNI). In the present study, end-to-end neurorrhaphy (EEN) was performed using an in vivo model of PNI. The distribution of K^+ at regenerating axons following EEN was detected by time-of-flight secondary-ion mass spectrometry. The specific localization and expression of Kv1.1/Kv1.2 channels were examined by confocal microscopy and western blotting. Our data showed that the re-establishment of K^+

distribution and intensity was correlated with the functional recovery of compound muscle action potential morphology in EEN rats. Furthermore, the re-clustering of Kv1.1/1.2 channels 1 and 3 months after EEN at the nodal region of the regenerating nerve corresponded to changes in the K^+ distribution. This study provided direct evidence of K^+ distribution in regenerating axons for the first time. We proposed that the Kv1.1/Kv1.2 channels re-clustered at the JXP regions of regenerating axons are essential for modulating the proper patterns of K^+ distribution in axons for maintaining membrane potential stability after EEN.

Keywords Voltage-gated potassium channels (Kv channels) · Kv1.1 · Kv1.2 · End-to-end neurorrhaphy (EEN) · Juxtaparanodal region

Introduction

Peripheral nerve injury (PNI) is a major cause of disabilities and blocks signals from the spine to the extremities. Regeneration of damaged axons is a process involving demyelination, remyelination, and recovery of voltage-gated K^+ , Na^+ , and Ca^{2+} channels. Among these channels, the voltage-gated potassium channels (Kv channels) are redistributed on the regenerated axons, which is highly associated with myelination status (Boyle et al. 2001; Krishnan et al. 2009). However, the correlation between Kv channel distribution and changes of potassium ion intensity on regenerating axons has never been documented.

In the mammalian nervous system, each Kv channel contains four α subunits to form a tetrameric pore associated with four β subunits. There are 40 known α subunits of Kv in humans. According to sequence homology, the α subunits can be further divided into 12 subfamilies

✉ Wen-Chieh Liao
khrnangel@gmail.com

¹ Department of Anatomy, Faculty of Medicine, Chung Shan Medical University, No. 110, Sec. 1, Jianguo N. Rd, Taichung 40201, Taiwan

² Department of Pediatrics, Chung Shan Medical University Hospital, Taichung, Taiwan

³ Department of Anatomy and Cell Biology, School of Medicine, College of Medicine, Taipei Medical University, Taipei 11031, Taiwan

⁴ Department of Medical Education, Chung Shan Medical University Hospital, No. 110, Sec. 1, Jianguo N. Rd, Taichung, Taiwan

(Kv1–Kv12). All Kv channels are activated upon depolarization of the plasma membrane, restoring the neuronal resting membrane potential (Gutman et al. 2005). In peripheral nerves, high-density clustering of Kv1 channels (Shaker potassium channels) is found in the juxtaparanodal (JXP) regions of myelin axons, whereas only low-density clustering of Kv1 is present in the internode (Roper and Schwarz 1989; Wang et al. 1993). The most prevalent combination of Kv1.1 and Kv1.2 channels is presented at the JXP regions as an exclusive membrane domain for the Kv conductance responsible for the rapid axonal repolarization in mammals. Both Kv1.1 and Kv1.2 channels are considered low-voltage-activated channels, which activate with small depolarizations at or below resting potential. Therefore, the distinct distribution and biophysical properties of Kv1.1/Kv1.2 channels contribute to potassium ion concentration regulation in the axons, and they are necessary for the maintenance of a stable nodal resting potential (Barrett and Barrett 1982; Waxman and Ritchie 1993; Krishnan et al. 2009; Chiu and Ritchie 1984).

After peripheral nerve injury, myelin disruption increases exposure of Kv1.1 channels on axons, which in turn may lead to a decrease in action potential amplitude and duration due to the clamping of the resting membrane potential close to the K^+ equilibrium potential (Waxman and Ritchie 1993; Krishnan et al. 2009). Additionally, it has been proposed that demyelination of intact axons by disease or injury leads to diffusion of Kv1 channels rather than clustered sodium channels (Poliak and Peles 2003). The misplaced Kv1 channels result in an increase in paranodal capacitance and a decrease in resistance, consequently hampering the propagation of action potentials (Boyle et al. 2001; Krishnan et al. 2009). In clinical tests, Kv1 dysfunction results in neuronal channelopathies associated with neurological disorders, including neuromyotonia, Morvan's syndrome, limbic encephalitis, forms of epilepsy, and episodic ataxia type 1 (Browne et al. 1994; Irani et al. 2010; Glasscock et al. 2010; Diani et al. 2008; Zuberi et al. 1999).

Although the functional distribution and combinations of Kv1 on myelin axons have been investigated, the direct correlation between redistributed Kv1 and potassium ion intensity changes on a regenerating axon has never been examined. In this study, we used end-to-end neurorrhaphy (EEN) of musculocutaneous nerves (McN) to ulnar nerves (UN), which provided a stable and reproducible peripheral nerve regeneration model for analysing Kv1.1/Kv1.2 distribution and expression (Liao et al. 2009, 2010, 2013; Liu et al. 2016; Chang et al. 2014). Because traditional potassium indicator assays are only able to detect cytosolic free potassium ions, intracellular potassium concentrations cannot be evaluated. To overcome this obstacle, time-of-flight secondary-ion mass spectrometry (TOF-SIMS) was used in this study. TOF-SIMS is a high-sensitivity technique used

to measure both the distribution and intensity of unlabelled ions in tissue samples (Liu et al. 2016; Kulp et al. 2006).

Materials and methods

Experimental animals

Young adult male Wistar rats weighing 200–300 g ($n = 30$) were obtained from the Laboratory Animal Center of the Chung Shan Medical University and were used in this study. All experimental animals were housed under similar conditions with controlled temperature and humidity. All experimental procedures with surgical intervention were approved by the Laboratory Animal Center Authorities of the Chung Shan Medical University (IACUC Approval No 1658).

Surgical procedures

The in vivo model of PNI was performed using end-to-end neurorrhaphy (EEN) as described in our previous studies (Chang et al. 2013; Liao et al. 2009, 2010). Briefly, after the rats were deeply anaesthetized with an intraperitoneal injection of 7% chloral hydrate (Sigma-Aldrich, St. Louis, MO, USA), they were placed on a surgical microscope, and an incision was made along the left mid-clavicular line to expose the left brachial plexus. The musculocutaneous nerve (McN) was then transected at the margin of the pectoralis major muscle. The end of the proximal ulnar nerve (UN) was then neurorrhaphied to the end of the distal McN (Oberlin et al. 1994) with 10-0 nylon sutures (Ethilon, Edinburgh, UK) under the surgical microscope. The wound was closed with 5-0 silk, and the animals were monitored for 1–3 months following surgery. All operated animals were divided into three groups with ten individuals per group. A sham operation was performed in Group I by exposing the brachial plexus. Group II (EE1M group) and Group III (EE3M group) were treated with end-to-end neurorrhaphy for 1 and 3 months, respectively.

Compound muscle action potential recording

To confirm nerve reconstruction recovery, compound muscle action potentials (CMAPs) of the repaired nerve and target muscle were recorded with a PowerLab electromyogram (AD instrument, Sydney, Australia). First, the experimental animals were anaesthetized. The stimulating electrode was placed above the reconnection site, and the recording electrode was placed in the biceps brachii muscle at the mid-humerus level. The recording electrode was kept 1 cm from the stimulating electrode with a piece of 5-0 nylon suture. The rat's tail was connected to the

signal ground. Next, the nerve was stimulated with a 0.2 ms square pulse current in 2 mA at a repetition rate of 0.2 Hz. In sham-operated rats, electrodes were set at corresponding locations of the McN and biceps brachii muscle. Data were then digitized and analysed.

Perfusion and tissue preparation

To perform TOF-SIMS and immunofluorescence, at the end of the survival period after EEN, half of the experimental animals from all groups were deeply anaesthetized with 7% chloral hydrate (0.4 mL/100 g) and subjected to transcardiac perfusion with 100 mL of Ringer's solution followed by 45 min of fixation with 4% paraformaldehyde in 0.1 M phosphate buffer (PB), pH = 7.4. After perfusion, the distal end of the repaired nerve was removed under a dissecting microscope and kept in a similar fixative for 2 h. The tissue block was then immersed in graded concentrations of sucrose buffer (10–30%) for cryoprotection at 4 °C overnight. Serial 25- μ m-thick sections of the nerve segment were cut longitudinally with a cryostat (CM3050S, Leica Microsystems, Wetzlar, Germany) the following day. For immunoblotting, the other half of the deeply anaesthetized experimental animals were perfused with Ringer's solution, and then the musculocutaneous nerves were quickly removed under a dissecting microscope. The samples were stored at -80 °C until use.

Kv1 channel and PGP 9.5 immunofluorescence stain

For Kv1 channels and PGP 9.5 immunohistochemistry, the collected tissue sections were first placed in a blocking medium containing 0.1% Triton X-100, 3% normal goat serum, and 2% bovine serum albumin (all from Sigma-Aldrich, St. Louis, MO, USA) for 1 h to block nonspecific binding. After several washes in phosphate-buffered saline (PBS), the sections were incubated in rabbit polyclonal anti-Kv1.1 antibody (1:100, Alomone Laboratories, Jerusalem, Israel), rabbit polyclonal anti-Kv1.2 antibody (1:100, Alomone Laboratories, Jerusalem, Israel), and mouse polyclonal PGP 9.5 antibody (1:500, Eugene, OR, USA) with the blocking medium for 24 h at 4 °C. After incubation in primary antibodies, the sections were further incubated with Alexa Fluor anti-mouse IgG (1:200, Jackson Immuno-Research, West Grove, PA, USA) and Cy3-conjugated anti-rabbit IgG (1:200, Jackson Immuno-Research, West Grove, PA, USA) to visualize PGP 9.5 and Kv1 channels, respectively. All mounted sections were examined and photomicrographed under a confocal fluorescence microscope (SP5, Leica Microsystems, Wetzlar, Germany). The Z-stacked confocal images of the nerve were captured with a confocal microscope (TCS SP5) to analyse the Kv1.1/Kv1.2 distribution and recovery of the repaired nerve. Each

confocal photomicrograph is created using a stacked series of scans of a nerve Section (25 μ m in total thickness). The z-stack images were captured from regenerating axons (5 μ m optical slice thickness, 10 z-sections collected at 0.486- μ m intervals).

Western blotting

Musculocutaneous nerve tissue samples were subjected to western blot analysis. Three tissue samples of distal McN removed from the suture site of each group was first homogenized with Kaplan buffer (50 mM Tris buffer, pH = 7.4, 150 mM NaCl, 10% glycerol, 1% NP40, and protease inhibitor cocktail) and then clarified by centrifugation. Then, equal amounts of solubilized proteins and cell lysates were separated on SDS-PAGE (10%) and electroblotted onto nitrocellulose membranes (Bio-Rad Laboratories, Hercules, CA, USA). The membranes were then blocked with 5% skim milk and probed with antibodies against β -actin (1:10,000, BD Biosciences, San Jose, CA, USA), Kv1.1 (1:1000, Alomone Laboratories, Jerusalem, Israel), Kv1.2 (1:1000, Alomone Laboratories, Jerusalem, Israel), and PGP 9.5 (1:500, Abcam, Cambridge, UK) at 4 °C overnight. After incubation with primary antibodies, the membranes were incubated with horseradish peroxidase-conjugated secondary antibodies (Bethyl Laboratories, Montgomery, TX, USA) at a dilution of 1:10,000 for 1 h at room temperature. ECL solutions (Millipore, Temecula, CA, USA) were used to detect the signals generated.

In the present study, we normalized the Kv1.1 and Kv1.2 protein to PGP 9.5 protein to adjust for changes in the axonal number as previously described (Calvo et al. 2016).

TOF-SIMS analysis

TOF-SIMS analysis was carried out on a TOF-SIMS IV instrument (ION-TOF GmbH, Munster, Germany). For ionic image analysis, the 25- μ m-thick cryostat sections of repaired MCN were mounted on the silicon wafer pieces and air-dried for the TOF-SIMS IV instrument. Serial sections were observed and images of them captured by differential interference contrast (DIC) microscopy (Axioskop 2 plus, Zeiss, Göttingen, Germany). A gallium (Ga^+) ion gun operated at 25 kV was used as the primary ion source (1 pA pulse current) for experiments conducted during this study. The Ga^+ primary ion beam scanned an area of 100 μm^2 . Positive secondary ions passing through a reflectron mass spectrometer were detected with a micro-channel plate assembly operating at 10 kV postacceleration. Mass calibration of the ion spectrum was achieved using a set of mass peaks such as $m/z = 15$ (CH_3^+), 41 (C_3H_5^+), and 69 (Ga^+), and a paraformaldehyde molecule since this element was the major component in the tissue matrix following

vascular fixation (Chang et al. 2012). The ions related to K^+ ($m/z = 39$) were used to identify and evaluate the molecular image of potassium expression.

Statistical analysis

For TOF-SIMS analysis, the spectral intensity detected from each section was normalized to the ion intensity of paraformaldehyde (serving as base line = 100%) and was expressed as the percentage above the base line (Chang et al. 2012). All quantitative data acquired from spectrometry, immunofluorescence, and immunoblotting in sham-operated and EEN rats were subjected to Student's *t* test. Data were presented as the mean \pm SD. $P < 0.05$ was considered statistically significant.

Results

Expression of Kv1.1/Kv1.2 channels after end-to-end neurorrhaphy

Maintaining the concentration of potassium ions at the JXP region of the nerve is essential for limiting re-excitation and promoting saltatory conduction. It is known that both Kv1.1 and Kv1.2 channels are associated with anchoring proteins on the cell membrane. These complexes link cytoskeleton to extracellular matrix constituents and stabilize the structure of the nodal area (Fig. 1a), whereas disrupted myelination could potentially alter Kv1 channel localization and expression levels (Fig. 1b) (Barrett and Barrett 1982; Waxman and Ritchie 1993; Krishnan et al. 2009). To examine this observation in our EEN animal model, regenerated nerves were analysed at 1 and 3 months post-surgery. The distal ends of regenerating nerve fibres were stained with protein gene product 9.5 (PGP 9.5). This product is often used as a marker to identify neural profiles and axon regeneration. Confocal microscopy revealed that the axon is reduced in diameter in certain areas and the location of node of Ranvier (Hess and Young 1952; King 2013). As expected, in the sham-operation group, Kv1.1 and Kv1.2 channels were concentrated at the JXP regions (Figs. 2 and 3). One month after EEN, expression of Kv1.1 and Kv1.2 channels appears to have a widespread distribution across the regenerated axons. Three months post-surgery, Kv1.1 and Kv1.2 channels assembled and congregated again at the JXP regions on the regenerated axons (Figs. 2 and 3). These results indicate that the dislocation of Kv1.1 and Kv1.2 on regenerating axons in our EEN model is similar to the process described in previous studies.

We further quantified Kv1.1 and Kv1.2 expression on regenerating axons using western blots. The results showed that the expression of Kv1.1 and Kv1.2 was up-regulated

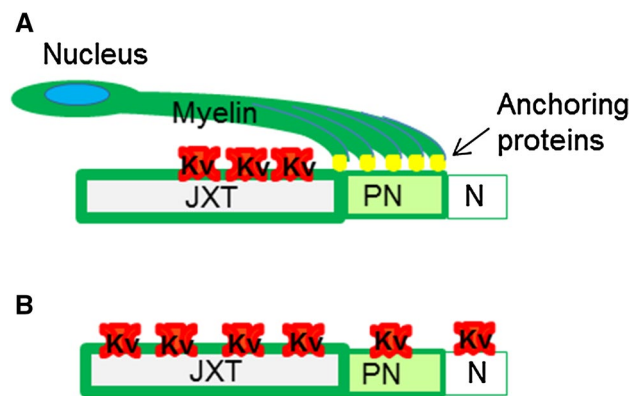


Fig. 1 Diagram illustrating the structure of the myelinated nerve fibre and axonal domains: Nodes of Ranvier (N), paranode (PN), and juxtaparanodes (JXP). **a** Schematic presentation showing the high density of Kv1 channel distribution at JXP covered by a myelin sheath. **b** Disruption of myelination occurs with nerve injury, resulting in the loss of anchoring proteins and displacement of the innermost myelin contacts that permit the movement of Kv channels dispersed along the axon

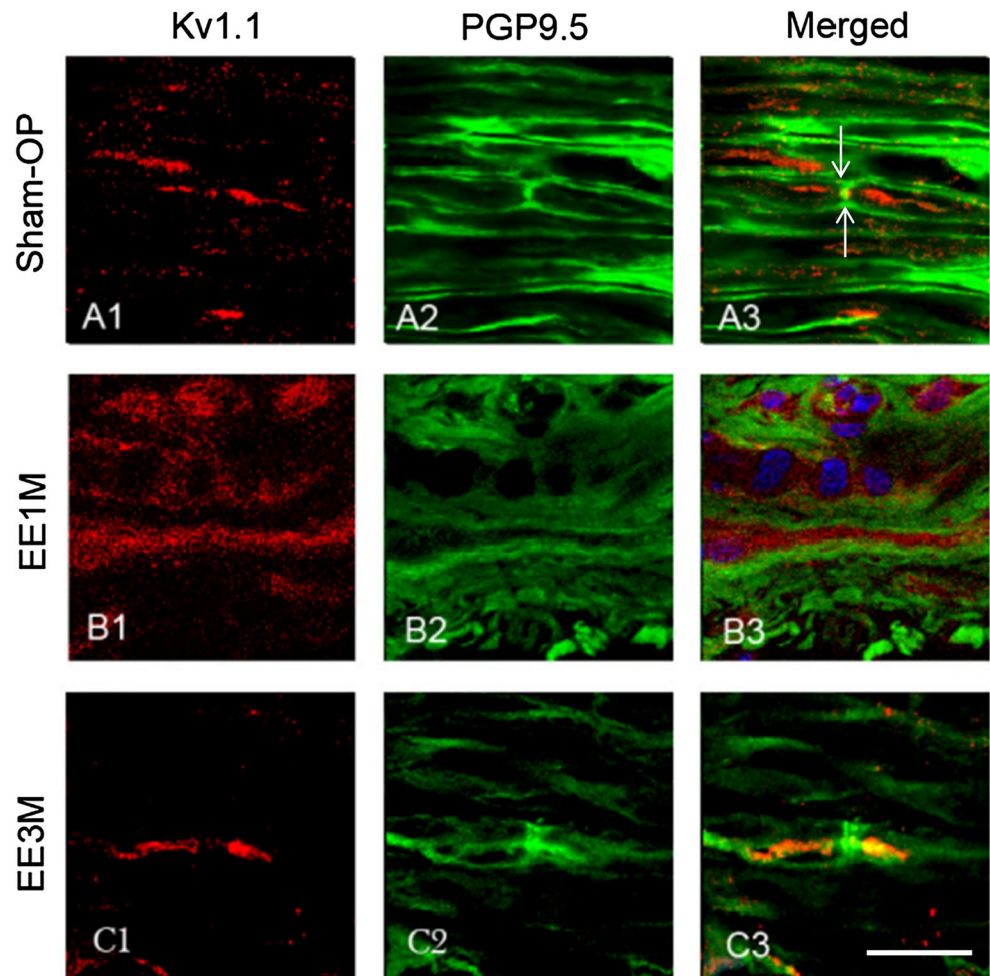
at repaired nerves 1 month after EEN (Figs. 4a, 5a). At 3 months after EEN, expression of Kv1.1 and Kv1.2 was decreased in the regenerating nerve compared to that in the 1-month EEN tissue, but still higher than that in the sham-operation group (Figs. 4b, 5b).

Ion mapping of repaired nerve after EEN by time-of-flight secondary-ion mass spectrometry

To determine the correlation between potassium ion distribution and the expression of Kv1.1 and Kv1.2 channels on regenerating axons, we analysed nerve tissue by TOF-SIMS. TOF-SIMS showed the *in vivo* ionic images of potassium distribution as well as the normalized spectral intensity of potassium ions on tissue slides. The results showed that strong potassium ion signals were concentrated at the peri-nodal region of the sham-operation axons (Fig. 6a). One month following EEN, the potassium ion signals were not concentrated at the peri-nodal region of the regenerating nerve. Instead, dispersed potassium ion signals were observed along the axons. At 3 months following EEN, most of the potassium ions were concentrated at the peri-nodal region again. This result revealed a re-establishment of potassium ions distribution on regenerating axons during the recovery process after EEN. The absolute counts of potassium ions on the nerve tissue were normalized to the total paraformaldehyde ions. We found that the quantity of potassium ions significantly increased 1 month after EEN and then decreased to equivalent levels relative to the sham-operation group at 3 months (Fig. 6b, c).

To ensure that the recovery of Kv1 channels and potassium ions correspond with nerve functions, CMAP analysis

Fig. 2 Confocal photomicrographs showing the distribution of Kv1.1 channels and PGP 9.5 in longitudinally regenerating axons. The recipient nerve tissues (distal end of McN) were immunostained with anti-PGP 9.5 mAb (green) and anti-Kv1.1 polyclonal antibody (red) 1 and 3 months following EEN. At the node of Ranvier, the axon is reduced in diameter; the arrow **a3** indicates the narrow portion of a PGP 9.5-positive axon. Representative images are shown. The distribution of Kv1.1 channels was concentrated in the JXP region (Fig. **a1**, **a3**), whereas Kv1.1 channels were scattered throughout the regenerating nerve fibres 1 month following EEN (Fig. **b1**, **b3**). Note that Kv1.1 channels underwent a structural rearrangement at the JXP region 3 months following EEN (Fig. **c1**, **c3**). Scale bar = 20 μ m



was performed. One month after surgery, the action potential of the EEN group still generated both a long duration and low amplitude in comparison to the sham-operation group. At the end of the third month, the electrophysiological recordings showed that the regenerated axons of the EEN group successfully re-innervated the target muscles and generated CMAPs (3.9 ± 0.3 mV in EE3M and 3.8 ± 0.1 mV in sham-operation group; Fig. 7a, b). In addition, the response duration of CMAP in the EE3M group (2.51 ± 0.11 ms) improved to the control level of the sham-operation group (2.50 ± 0.10 ms; Fig. 7c).

Discussion

The present study was the first to report the potassium ion distribution and its correlation with Kv1.1 and Kv1.2 expression in a distal segment of regenerating axon following EEN. The potassium ion signals were shown in terms of both ionic imaging and normalized spectrometric quantity.

We found that the up-regulation of Kv1.1 and Kv1.2 on the axon coincided with high potassium ion intensity along regenerating axons 1 month after EEN. In addition, the diffused expression of Kv1.1 and Kv1.2 channels along the axon is tightly associated with dispersed potassium ion distribution. Moreover, the reappearance of clustered Kv1.1 and Kv1.2 at the peri-nodal region highly corresponded with the re-concentrated potassium ion signals 3 months after EEN.

Measurement of tissue potassium in vivo

Potassium (K^+) is a major ionic constituent within cells. Fluctuations in intracellular K^+ concentrations are associated with a wide range of physiological effects. Previous methods for measuring tissue K^+ concentrations have involved plasma and whole blood counting techniques or fluorescence tracer studies (e.g., potassium indicator assays) (Fijorek et al. 2014). All these methods differ in their accuracy and limits of detection. Because

Fig. 3 Confocal photomicrographs showing the distribution of Kv1.2 channels and PGP 9.5 in longitudinally regenerating axons. The recipient nerve tissues (distal end of McN) were immunostained with anti-PGP 9.5 mAb (green) and anti-Kv1.2 polyclonal antibody (red) 1 and 3 months following EEN. At the node of Ranvier, the axon is reduced in diameter; the arrow **a3** indicates the narrow portion of the PGP 9.5-positive axon. Representative images are shown. The distribution of Kv1.2 channels was concentrated in the JXP region (Fig. **a1, a3**), whereas Kv1.2 channels were scattered throughout the regenerating nerve fibres 1 month following EEN (Fig. **b1, b3**). Note that Kv1.2 channels underwent a structural rearrangement at JXP region 3 months following EEN (Fig. **c1, c3**). Scale bar = 20 μ m

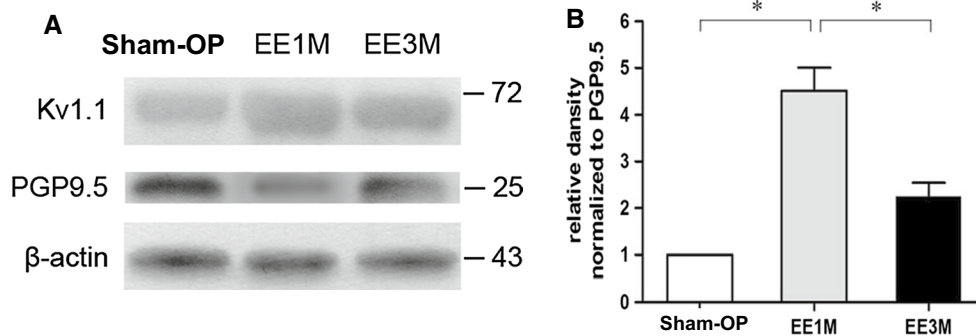
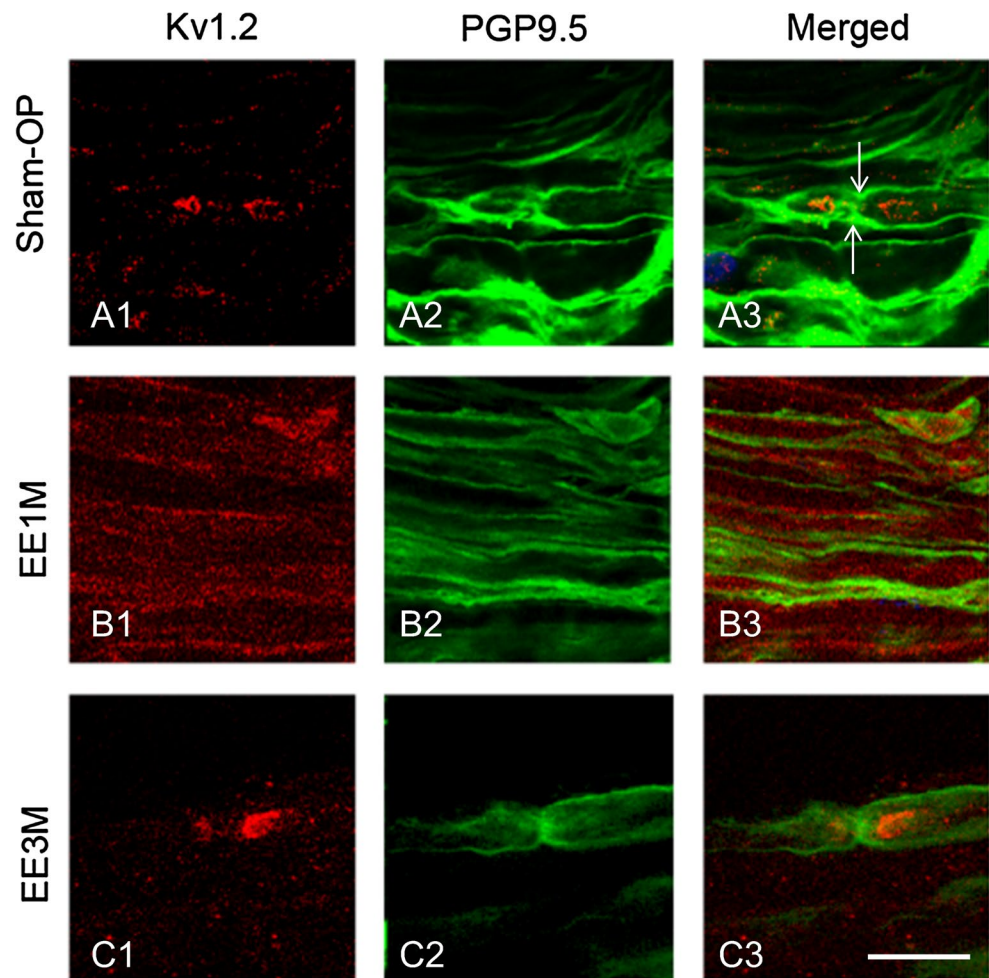


Fig. 4 Immunoblot (**a**) and histogram (**b**) showing Kv1.1 expression in nerve tissues of normal and 1- to 3-month EEN rats. Expression of PGP 9.5 (24 kDa) and Kv1.1 (72 kDa) was detected. β -actin was used as a loading control (**a**). Densitometric analysis indicated a higher ratio of Kv1.1 to PGP 9.5 in the EE1 M groups compared to the sham-op group (**b**). Target band detection was normalized against

PGP 9.5 correspondingly for analysis. The Kv1.1 expression in the EE1M group was 4.3-fold higher than that in the sham-op group. Furthermore, the EE3M group showed a 2.1-fold increase in the ratio of Kv1.1 to PGP 9.5 (Fig. **1b**). Data are present as mean \pm SD from three independent experiments. * $P < 0.05$

98% of whole-body potassium is intracellular, measurements of plasma K^+ concentrations are often a very insensitive index of tissue K^+ stores (Kernan 1980). K^+

measurement with fluorescence probes cannot be used to measure in vivo tissue and are not directly obtained from the data immediately. TOF-SIMS analysis provides mass

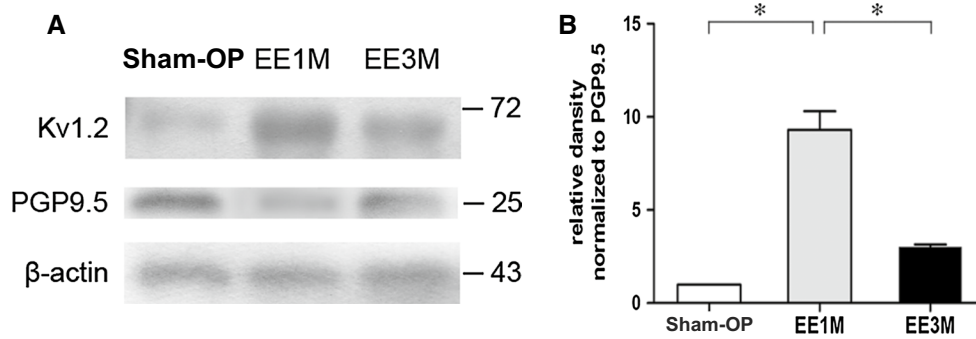


Fig. 5 Immunoblot (a) and histogram (b) showing Kv1.2 expression in nerve tissues of normal and 1- to 3-month EEN rats. Expression of PGP 9.5 (24 kDa) and Kv1.2 (72 kDa) was detected. β -actin was used as a loading control (a). Densitometric analysis indicated a higher ratio of Kv1.2 to PGP 9.5 in the EE1M groups compared to the sham-op groups (b). Target band detection was normalized against PGP

9.5 correspondingly for analysis. The Kv1.2 expression in the EE1M group was 8.0-fold higher than that in the sham-op group. Furthermore, the EE3M group showed a 3.1-fold increase in the ratio of Kv1.2 to PGP 9.5 (Fig. 1b). Data are present as mean \pm SD from three independent experiments. * $P < 0.05$

spectral and image information present on the tissue sample even when tissue samples are not previously stained and handled. This technique was useful for clinical diagnosis as well as for investigating and generating imagery of K^+ on the tissue surface.

Redistribution of potassium ion correlated with Kv1 channels expression after end-to-end neurotaphy

It is well known that the transduction of proper action potential relies on appropriate ion channel distribution along axons (Lai and Jan 2006). The potassium ion concentration is higher inside the axons, while the sodium ion concentration is higher outside the axons at rest. Potassium ion fluctuations in mammalian myelinated axons are restricted to the JXP region, where voltage-gated Kv1.1 and Kv1.2 channels are clustered at a particular high density. This structural organization limits axonal hyperexcitability with brief action potentials (Calvo et al. 2016). TOF-SIMS showed that the distribution of potassium ions was clustered at the perinodal region of normal nerve tissue. During the first month after EEN, we observed the expression pattern of potassium ions and Kv1.1/Kv1.2 channels, which dispersed along the regenerating nerve. We suggested that these Kv1 channel dispersions could facilitate hyperpolarization of potassium ion efflux across the plasma membrane and counteract inward ion conductance. Therefore, this process could result in equal concentrations of potassium ions inside and outside of axons and thus limit neuronal excitability. Furthermore, the ionic imaging illustrated that the redistribution K^+ concentrated and re-clustered with Kv1 channels at the peri-nodal region of EEN3M-rats (Fig. 6).

Injury to the peripheral nervous system could cause disorganization of Kv1 channel distribution, leading to co-localization with nodal Na^+ channels and disruption of the paranode in demyelinated axons (Arroyo et al. 1999; Rasband 2004; Rasband et al. 1998). Since the diffuse localization of Kv1.1 and Kv1.2 channels exposed at the node and paranode leads to increased activity of the Kv1 channel, it may approach the K^+ equilibrium potential, reducing membrane excitability and blocking conduction (Nashmi and Fehlings 2001). Interestingly, the alteration of Kv1.1/Kv1.2 density at the JXP region depends on the degree of remyelination, which correlates to the extent of axonal regeneration observed in this study.

Electrophysiological recovery in regenerating nerve

The function of Kv1 channels is critically dependent on their ability to target specific neuronal compartments. In normal nerves, the Kv channels Kv1.1 and Kv1.2 are present at juxtaparanode to regulate nodal excitability and conduction (Rasband et al. 1998; Calvo et al. 2016). During the regenerative process of PNI, the exposure of Kv1 channels at the nodal region caused spreading potassium ions to damage impulse conduction (Vabnick et al. 1999). In this study, the EE1 M group exhibited longer duration and weaker amplitude of CMAP, which corresponded to the dispersed Kv1.1 and Kv1.2 staining pattern and potassium ion redistribution. Previous studies showed that misplaced potassium expression at the nodal region could not easily cause repolarization of the membrane potential (Calvo et al. 2016; Foust et al. 2011). The dispersed potassium ions at the regenerating nerve

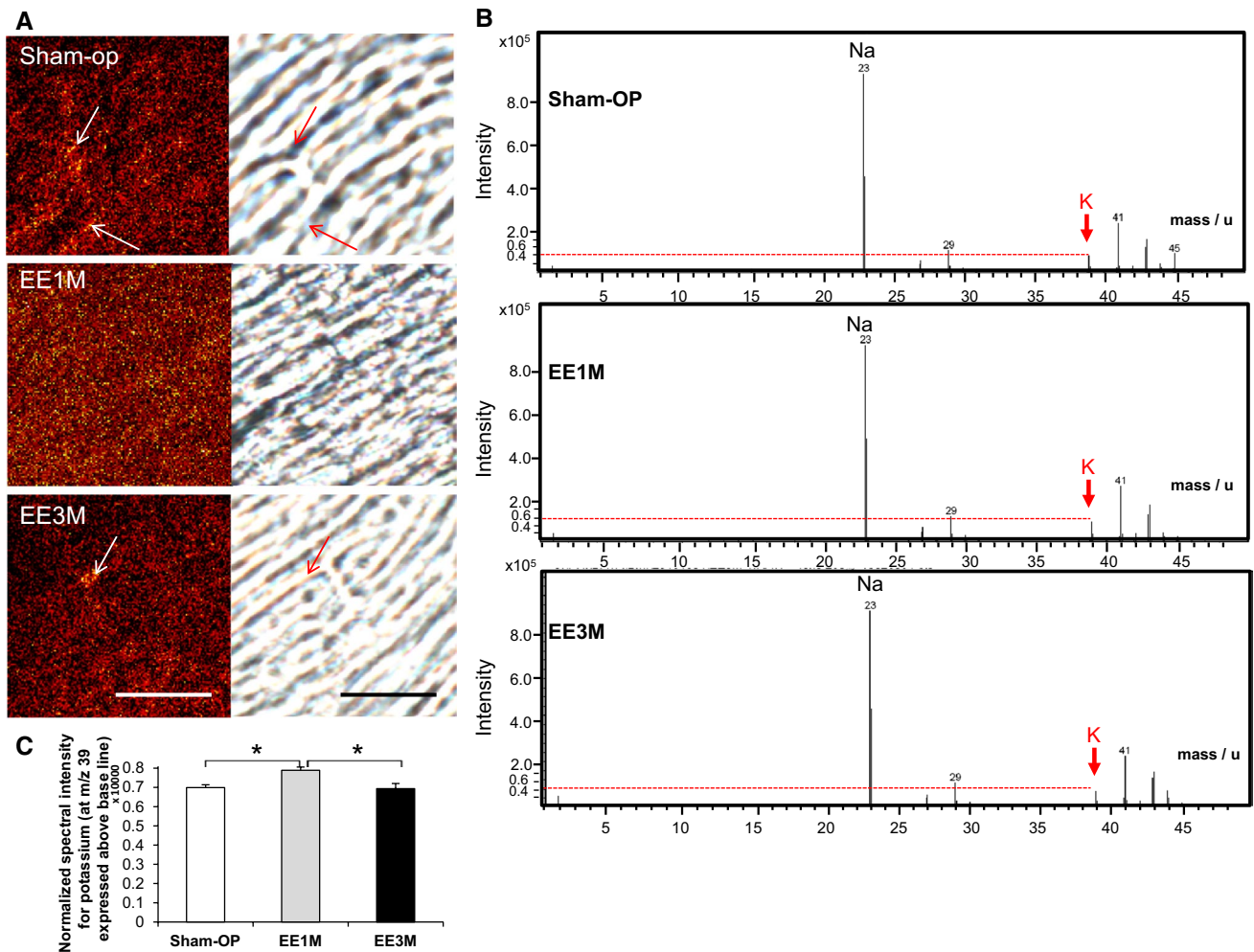


Fig. 6 TOF-SIMS images of regenerating axons. **a** Ionic images of potassium (*left column*) and corresponding DIC bright filed images (*right column*) on the serials longitudinal sections of repaired nerve from sham operation (Sham-OP), 1 and 3 months after EEN groups were shown. Cryosectioned nerves were air-dried and then analysed by TOF-SIMS. The K^+ images were scanned over an area of $100 \mu\text{m}^2$. Bright colours (*arrow*) represent high intensity of ions. *White arrows* indicate potassium-concentrated spots on the axons, and *red arrows* indicate the location of spots on DIC images. Note

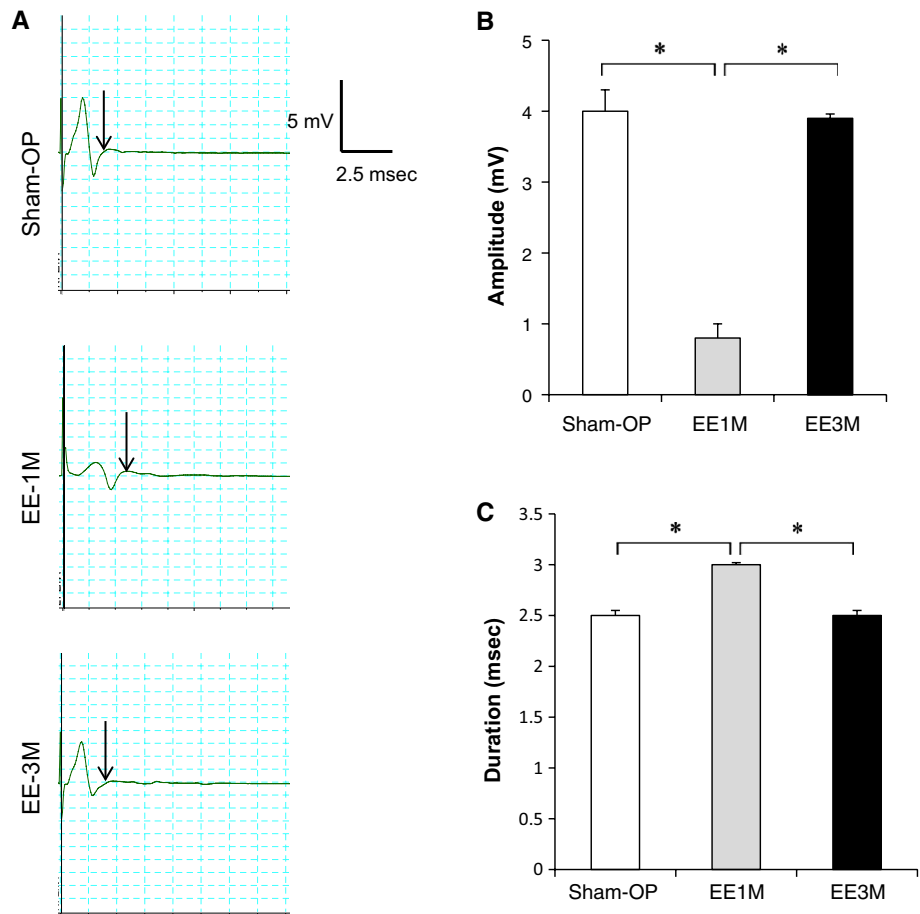
that potassium-concentrated spots appeared segmentally in the Sham-OP group, dispersed in the EE1M group, and partly reappeared in EE3M group. Representative photographs are shown. *Scale bar* = $50 \mu\text{m}$. **b** TOF-SIMS positive spectra (from 1–50 *m/z*) of Sham-OP, EE1M, and EE3M are shown. **c** The nerve sections revealed the intensity of potassium (*m/z* 39) after normalization to the total paraformaldehyde ions of each analysis. Note that normalized K^+ intensity increased in the EE1M group and recovered in the EE3M group. $N = 10$ for each group. * $P < 0.05$

had also been correlated with excitability abnormalities, which might prolong the duration of action potential and could not exert normal conduction velocities. The EE3M group displayed shorter CMAP duration and greater amplitude corresponding to the re-concentrated Kv1.1 and Kv1.2 staining patterns and re-clustered potassium ion distributions at the juxtapanode region. Our findings provide a better understanding of the interaction between the Kv1 channel and potassium ions in explaining the dynamics of action potential propagation. Examining the interactions between Kv1 and K^+ in the

regenerating nerves may provide a useful potential indicator for evaluating the outcome of PNI.

In conclusion, we suggest that dynamic changes in the re-arrangement Kv1.1/Kv1.2 channel could regulate effluxes of potassium ions at the JXP regions of the regenerating axon, thus contributing to the electrical stability of the nodal potential. Therefore, we support using potassium channel blockers, such as Fampridine, to improve slow nerve conduction velocity in patients suffering PNI (Wulff et al. 2009). The obtained information will not only improve our understanding of Kv1.1/Kv1.2 channels in the

Fig. 7 The recovery of compound muscle action potentials (CMAPs) after EEN. The responses were recorded from biceps brachii muscle upon activation of the nerve. The representative responses recorded from the sham-op group (*upper row*) and 1 and 3 months (*lower row*) following end-to-end neurorrhaphy are illustrated. The *arrow* indicates the end of the duration. Stimuli at moderate (2 mA) strengths were applied to the nerve above the neurorrhaphy site. Histograms **b** and **c** show the averages of amplitude and duration, respectively. $N = 10$ for each group. Values are the mean \pm SD. $*P < 0.05$ compared to that of sham-op value



initial stage of nerve regeneration but also provide insights into Kv1 channels targeting drugs for the clinical usage of PNI.

Acknowledgements This study was supported by research grants to Dr. W. C. Liao from the Ministry of Science and Technology (MOST-105-2320-B-040-029-MY3). Cryostatting (CM3050S, Leica 149 Microsystems) was performed in the Instrument Center of Chung Shan Medical University, which was supported by Ministry of Science and Technology, Ministry of Education, and Chung Shan Medical University.

Compliance with ethical standards

Conflict of interest The authors have declared that no conflict of interest exists.

References

- Arroyo EJ, Xu YT, Zhou L, Messing A, Peles E, Chiu SY, Scherer SS (1999) Myelinating Schwann cells determine the internodal localization of Kv1.1, Kv1.2, Kvbeta2, and Caspr. *J Neurocytol* 28(4–5):333–347
- Barrett EF, Barrett JN (1982) Intracellular recording from vertebrate myelinated axons: mechanism of the depolarizing after potential. *J Physiol* 323:117–144
- Boyle ME, Berglund EO, Murai KK, Weber L, Peles E, Ranscht B (2001) Contactin orchestrates assembly of the septate-like junctions at the paranode in myelinated peripheral nerve. *Neuron* 30(2):385–397
- Browne DL, Gancher ST, Nutt JG, Brunt ER, Smith EA, Kramer P, Litt M (1994) Episodic ataxia/myokymia syndrome is associated with point mutations in the human potassium channel gene, KCNA1. *Nat Genet* 8(2):136–140. doi:10.1038/ng1094-136
- Calvo M, Richards N, Schmid AB, Barroso A, Zhu L, Ivlic D, Zhu N, Anwandter P, Bhat MA, Court FA, McMahon SB, Bennett DL (2016) Altered potassium channel distribution and composition in myelinated axons suppresses hyperexcitability following injury. *eLife* 5:e12661. doi:10.7554/eLife.12661
- Chang HM, Liao WC, Sheu JN, Chang CC, Lan CT, Mai FD (2012) Sleep deprivation impairs Ca²⁺ expression in the hippocampus: ionic imaging analysis for cognitive deficiency with TOF-SIMS. *Microsc Microanal* 18(3):425–435. doi:10.1017/S1431927612000086
- Chang HM, Shyu MK, Tseng GF, Liu CH, Chang HS, Lan CT, Hsu WM, Liao WC (2013) Neuregulin facilitates nerve regeneration by speeding Schwann cell migration via ErbB2/3-dependent FAK pathway. *PLoS ONE* 8(1):e53444. doi:10.1371/journal.pone.0053444 (PONE-D-12-28118)
- Chang HM, Liu CH, Hsu WM, Chen LY, Wang HP, Wu TH, Chen KY, Ho WH, Liao WC (2014) Proliferative effects of melatonin on Schwann cells: implication for nerve regeneration following peripheral nerve injury. *J Pineal Res* 56(3):322–332. doi:10.1111/jpi.12125

- Chiu SY, Ritchie JM (1984) On the physiological role of internodal potassium channels and the security of conduction in myelinated nerve fibres. *Proc R Soc Lond B* 220(1221):415–422
- Diani E, Di Bonaventura C, Mecarelli O, Gambardella A, Elia M, Bovo G, Bisulli F, Pinardi F, Binelli S, Egeo G, Castellotti B, Striano P, Striano S, Bianchi A, Ferlazzo E, Vianello V, Coppola G, Aguglia U, Tinuper P, Giallonardo AT, Michelucci R, Nobile C (2008) Autosomal dominant lateral temporal epilepsy: absence of mutations in ADAM22 and Kv1 channel genes encoding LGI1-associated proteins. *Epilepsy Res* 80(1):1–8. doi:[10.1016/j.eplepsyres.2008.03.001](https://doi.org/10.1016/j.eplepsyres.2008.03.001)
- Fijorek K, Puskulluoglu M, Tomaszewska D, Tomaszewski R, Glinka A, Polak S (2014) Serum potassium, sodium and calcium levels in healthy individuals—literature review and data analysis. *Folia Med Cracov* 54(1):53–70
- Foust AJ, Yu Y, Popovic M, Zecevic D, McCormick DA (2011) Somatic membrane potential and Kv1 channels control spike repolarization in cortical axon collaterals and presynaptic boutons. *J Neurosci* 31(43):15490–15498. doi:[10.1523/JNEUROSCI.2752-11.2011](https://doi.org/10.1523/JNEUROSCI.2752-11.2011)
- Glasscock E, Yoo JW, Chen TT, Klassen TL, Noebels JL (2010) Kv1.1 potassium channel deficiency reveals brain-driven cardiac dysfunction as a candidate mechanism for sudden unexplained death in epilepsy. *J Neurosci* 30(15):5167–5175. doi:[10.1523/JNEUROSCI.5591-09.2010](https://doi.org/10.1523/JNEUROSCI.5591-09.2010)
- Gutman GA, Chandy KG, Grissmer S, Lazdunski M, McKinnon D, Pardo LA, Robertson GA, Rudy B, Sanguinetti MC, Stuhmer W, Wang X (2005) International Union of Pharmacology. LIII. Nomenclature and molecular relationships of voltage-gated potassium channels. *Pharmacol Rev* 57(4):473–508. doi:[10.1124/pr.57.4.10](https://doi.org/10.1124/pr.57.4.10)
- Hess A, Young JZ (1952) The nodes of Ranvier. *Proc R Soc Lond B* 140(900):301–320
- Irani SR, Alexander S, Waters P, Kleopa KA, Pettingill P, Zuliani L, Peles E, Buckley C, Lang B, Vincent A (2010) Antibodies to Kv1 potassium channel-complex proteins leucine-rich, glioma inactivated 1 protein and contactin-associated protein-2 in limbic encephalitis, Morvan's syndrome and acquired neuromyotonia. *Brain J Neurol* 133(9):2734–2748. doi:[10.1093/brain/awq213](https://doi.org/10.1093/brain/awq213)
- Kernan RP (1980) Cell potassium. Series vol 1, Wiley
- King R (2013) Microscopic anatomy: normal structure. *Handb Clin Neurol* 115:7–27. doi:[10.1016/B978-0-444-52902-2.00002-3](https://doi.org/10.1016/B978-0-444-52902-2.00002-3)
- Krishnan AV, Lin CS, Park SB, Kiernan MC (2009) Axonal ion channels from bench to bedside: a translational neuroscience perspective. *Prog Neurobiol* 89(3):288–313. doi:[10.1016/j.pneurobio.2009.08.002](https://doi.org/10.1016/j.pneurobio.2009.08.002)
- Kulp KS, Berman ES, Knize MG, Shattuck DL, Nelson EJ, Wu L, Montgomery JL, Felton JS, Wu KJ (2006) Chemical and biological differentiation of three human breast cancer cell types using time-of-flight secondary ion mass spectrometry. *Anal Chem* 78(11):3651–3658. doi:[10.1021/ac060054c](https://doi.org/10.1021/ac060054c)
- Lai HC, Jan LY (2006) The distribution and targeting of neuronal voltage-gated ion channels. *Nat Rev Neurosci* 7(7):548–562. doi:[10.1038/nrn1938](https://doi.org/10.1038/nrn1938)
- Liao WC, Chen JR, Wang YJ, Tseng GF (2009) The efficacy of end-to-end and end-to-side nerve repair (neurorrhaphy) in the rat brachial plexus. *J Anat* 215(5):506–521. doi:[10.1111/j.1469-7580.2009.01135.x](https://doi.org/10.1111/j.1469-7580.2009.01135.x)
- Liao WC, Chen JR, Wang YJ, Tseng GF (2010) Methylcobalamin, but not methylprednisolone or pleiotrophin, accelerates the recovery of rat biceps after ulnar to musculocutaneous nerve transfer. *Neuroscience* 171(3):934–949. doi:[10.1016/j.neuroscience.2010.09.036](https://doi.org/10.1016/j.neuroscience.2010.09.036)
- Liao WC, Wang YJ, Huang MC, Tseng GF (2013) Methylcobalamin facilitates collateral sprouting of donor axons and innervation of recipient muscle in end-to-side neurorrhaphy in rats. *PLoS ONE* 8(9):e76302. doi:[10.1371/journal.pone.0076302](https://doi.org/10.1371/journal.pone.0076302)
- Liu CH, Chang HM, Tseng TJ, Lan CT, Chen LY, Youn SC, Lee JJ, Mai FD, Chou JF, Liao WC (2016) Redistribution of Cav2.1 channels and calcium ions in nerve terminals following end-to-side neurorrhaphy: ionic imaging analysis by TOF-SIMS. *Histochem Cell Biol* 146(5):599–608. doi:[10.1007/s00418-016-1470-3](https://doi.org/10.1007/s00418-016-1470-3)
- Nashmi R, Fehlings MG (2001) Mechanisms of axonal dysfunction after spinal cord injury: with an emphasis on the role of voltage-gated potassium channels. *Brain research Brain research reviews* 38(1–2):165–191
- Oberlin C, Beal D, Leechavengvongs S, Salon A, Dauge MC, Sarcy JJ (1994) Nerve transfer to biceps muscle using a part of ulnar nerve for C5–C6 avulsion of the brachial plexus: anatomical study and report of four cases. *J Hand Surg Am* 19(2):232–237
- Poliak S, Peles E (2003) The local differentiation of myelinated axons at nodes of Ranvier. *Nat Rev Neurosci* 4(12):968–980. doi:[10.1038/nrn1253](https://doi.org/10.1038/nrn1253)
- Rasband MN (2004) It's "juxta" potassium channel! *J Neurosci Res* 76(6):749–757. doi:[10.1002/jnr.20073](https://doi.org/10.1002/jnr.20073)
- Rasband MN, Trimmer JS, Schwarz TL, Levinson SR, Ellisman MH, Schachner M, Shrager P (1998) Potassium channel distribution, clustering, and function in remyelinating rat axons. *J Neurosci* 18(1):36–47
- Roper J, Schwarz JR (1989) Heterogeneous distribution of fast and slow potassium channels in myelinated rat nerve fibres. *J Physiol* 416:93–110
- Vabnick I, Trimmer JS, Schwarz TL, Levinson SR, Risal D, Shrager P (1999) Dynamic potassium channel distributions during axonal development prevent aberrant firing patterns. *J Neurosci* 19(2):747–758
- Wang H, Kunkel DD, Martin TM, Schwartzkroin PA, Tempel BL (1993) Heteromultimeric K⁺ channels in terminal and juxtaparanodal regions of neurons. *Nature* 365(6441):75–79. doi:[10.1038/365075a0](https://doi.org/10.1038/365075a0)
- Waxman SG, Ritchie JM (1993) Molecular dissection of the myelinated axon. *Ann Neurol* 33(2):121–136. doi:[10.1002/ana.410330202](https://doi.org/10.1002/ana.410330202)
- Wulff H, Castle NA, Pardo LA (2009) Voltage-gated potassium channels as therapeutic targets. *Nat Rev Drug Discovery* 8(12):982–1001. doi:[10.1038/nrd2983](https://doi.org/10.1038/nrd2983)
- Zuberi SM, Eunson LH, Spauschus A, De Silva R, Tolmie J, Wood NW, McWilliam RC, Stephenson JB, Kullmann DM, Hanna MG (1999) A novel mutation in the human voltage-gated potassium channel gene (Kv1.1) associates with episodic ataxia type 1 and sometimes with partial epilepsy. *Brain J Neurol* 122(Pt 5):817–825